

The Color Glass Condensate and hadron production in the forward region

Adrian Dumitru^a, Arata Hayashigaki^a and Jamal Jalilian-Marian^b

^a*Institut für Theoretische Physik, J. W. Goethe Universität,
Max-von-Laue Strasse 1,
D-60438 Frankfurt am Main, Germany*

^b*Institute for Nuclear Theory, University of Washington, Seattle, WA 98195*

Abstract

We consider one loop corrections to single inclusive particle production in parton-nucleus scattering at high energies, treating the target nucleus as a Color Glass Condensate. We prove by explicit computation that in the leading $\log Q^2$ approximation, these corrections lead to collinear factorization and DGLAP evolution of the projectile parton distribution and hadron fragmentation functions. In single-inclusive cross sections, only two-point functions of Wilson lines in the adjoint and fundamental representations (Mueller's dipoles) arise, which can be obtained from the solution of the JIMWLK equations. The application of our results to forward-rapidity production shows that, in general, recoil effects are large. Hence, the forward rapidity region at RHIC is rather different from the central region at LHC, despite comparable gluon densities in the target. We show that both the quantum x -evolution of the high-density target as well as the DGLAP Q^2 -evolution of the parton distribution and fragmentation functions are clearly seen in the BRAHMS data. This provides additional strong evidence for the Color Glass Condensate at RHIC.

1 Introduction

The rapidity dependence of the recent RHIC data on hadron production in deuteron-gold collisions [1] may hint at the emergence of the Color Glass Condensate (CGC) [2] as the dominant physics in the forward rapidity region [3]. While the ratio of the hadron transverse momentum distributions in $d + Au$ versus pp collisions shows a Cronin enhancement at midrapidity and moderate transverse momentum [4], the enhancement turns into suppression as one goes to larger rapidities. The disappearance of the Cronin peak is most commonly taken to be due to the quantum evolution (with $\log 1/x$) of gluons in the target [5, 6, 7]. Another argument in favor of the CGC formalism is provided by the changing centrality dependence of the data as one goes to the forward region. Note also that leading-twist next-to-leading order perturbative QCD calculations [8] provide a good description of the inclusive distribution at forward rapidities in pp collisions but fail to describe the $d + Au$ BRAHMS h^- data by a conventional modification of the leading-twist parton densities in nuclei (shadowing). The CGC dynamics can be tested further by $p + A$ collisions at the LHC, where measurements in both the central and forward rapidity regions should be performed. Interestingly, particle production in the forward region of hadron-nucleus collisions also plays a key role for the properties of giant air showers from ultra-high energy cosmic ray interactions in the atmosphere [9]. Improving our understanding of particle production at large Feynman- x may therefore reveal the type and origin of those super-high energy particles.

Even though the qualitative predictions of the CGC were confirmed by the RHIC data, in order to firmly establish the CGC as the cause for the observed suppression of the hadron spectra in deuteron-gold collisions and to clarify the role of other scenarios [10] without $\log 1/x$ resummation, one needs to consider effects in the CGC framework which have been neglected so far and which may be significant. One such effect is the recoil of the source which radiates the produced gluons. Current approaches to gluon (hadron) production in proton-nucleus collisions [11, 12, 13] treat both the projectile proton and the target nucleus as a Color Glass Condensate, with the difference that the proton is assumed to be in the dilute regime while the target nucleus could be in either the dilute or dense regimes. This approach neglects recoil effects since only diagrams that survive in the $\xi \rightarrow 0$ limit, with ξ the momentum fraction of the produced gluon, are included. Gluon radiation and recoil effects should also be significant for the production of leading hadrons in deep-inelastic scattering from nuclei, where large distortions of the spectrum relative to leading-twist calculations have been predicted [14, 15].

However, in forward rapidity production of particles, the momentum fraction x of the projectile parton is large and treating the proton as a dilute CGC (i.e. subject to BFKL evolution [16]) can not be justified. Theoretically, BFKL resummation applies if the parameter $\alpha_s \log x_0/x \sim 1$, where $x_0 \sim 0.1$ is where the valence degrees of freedom reside. In order to gain appreciable longitudinal phase space so that BFKL evolution becomes significant, one needs to go much below x_0 , which is not the case in the forward rapidity region, where (by definition) the typical x in the proton wave function is of order x_0 . It is known from HERA data that the saturation scale of a proton reaches ~ 1 GeV only around

$x \sim 10^{-4}$. Since the saturation scale of the proton is so small (of order of Λ_{QCD}) at $x \sim x_0$, even the extended scaling regime is rather small, as well. The production of hadrons with $p_t \gg \Lambda_{QCD}$ in the forward rapidity region never receives any large contributions from either the saturation or the extended scaling regimes of the proton.

We therefore treat the projectile proton as a collection of quarks and gluons according to the parton model and consider scattering of these partons from the target nucleus, which is treated as a Color Glass Condensate. In Section 2 we consider one loop corrections to quark-nucleus scattering due to gluon radiation and show that recoil effects can be large. We then generalize this to include all processes at this order and show that in the leading $\log Q^2$ approximation, these lead to DGLAP evolution [17] of the quark and gluon distribution functions of the projectile proton, and of their fragmentation functions into hadrons. Thus, we prove explicitly that one can treat a high energy proton-nucleus collision as scattering of collinearly factorized partons (which evolve according to DGLAP evolution equation) in the proton on a dense nucleus treated as a Color Glass Condensate.

Furthermore, we show that the standard genuinely non-Abelian diagram where the produced gluon scatters from the saturated target field gives a contribution which decreases by a factor of two toward large rapidity. We then show that QED-like bremsstrahlung, which is usually disregarded, contributes about equally at large rapidity and “small” transverse momentum. Both contributions involve only two-point functions of Wilson lines (dipoles [18, 15]), in the adjoint and fundamental representations, respectively. This makes it possible to use the RHIC data on hadron production in $d + Au$ collisions to make predictions for electromagnetic processes such as photon and dilepton production [4, 19] since these electromagnetic processes also involve dipoles in the fundamental representation. The evolution of the target wave function with x can then be included by using the solution of the JIMWLK equations [2] for the dipole evolution (for first attempts see e.g. [20]) or alternatively, by using phenomenological parameterizations of the dipole profile.

Finally, we apply our results to forward rapidity hadron production in deuteron-gold collisions at RHIC energy. Lacking a solution of the JIMWLK equations we resort to the phenomenological parametrization of Kharzeev, Kovchegov and Tuchin for the dipole profile [6]. We find that the BRAHMS data can be reproduced with a p_t -independent K -factor. We show that both the DGLAP Q^2 -evolution of the distribution and fragmentation functions as well as the quantum x -evolution of the high-density target (anomalous dimension of its gluon distribution function) are clearly seen in the data. In our opinion, this strengthens the evidence for the Color Glass Condensate in high-energy $d + Au$ collisions [21] substantially.

Despite the rather good description of the data provided by the above-mentioned formalism, some words of caution may be in order. It has been shown within the NLO pQCD framework that at RHIC energy, incoherent leading-twist interactions with partons from the nucleus about $x_A \sim 0.01$ contribute significantly [8] (in fact, even overshooting the data at forward rapidity). While the contribution from this region can be neglected when very small x in the nucleus become accessible at very high energies, at RHIC energy it might be necessary to think about additional mechanisms which suppress such interactions [22]. In this paper we do not construct any such model, however, but assume the validity of the

high-energy approximation inherent in the non-linear x -evolution, namely that the target fields at rapidities below that of the probe can be integrated out to yield the effective saturation scale $Q_s(y)$. We return to this point in appendix B, where we show that the $2 \rightarrow 1$ like kinematics which arises in the high-energy limit probes very small momentum fractions in the target nucleus, on the order of $\langle x_A \rangle \sim 10^{-3}$ for hadrons produced at rapidity $Y \simeq 3.2$ (BRAHMS) and $\langle x_A \rangle \sim 10^{-4}$ for $Y \simeq 4$ (STAR).

2 Including recoil in gluon production

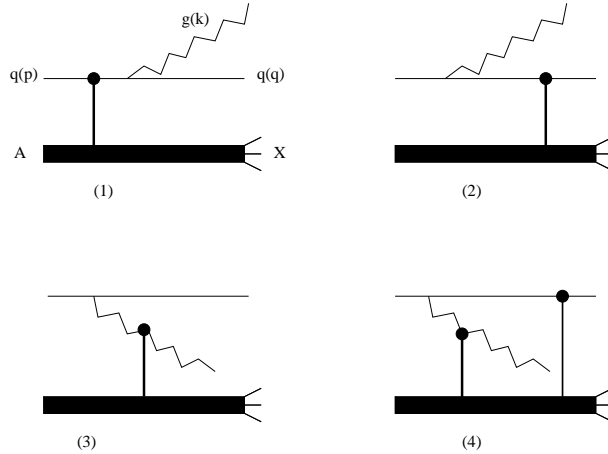


Figure 1: Diagrams contributing to gluon production in quark-nucleus scattering.

The diagrams contributing to gluon production in quark-nucleus scattering are shown in Fig. 1. The amplitudes for production of a massless quark with momentum q and a gluon with momentum k are given in [23] and read

$$\begin{aligned}
M_1 &= -ig \frac{1}{2q \cdot k} \bar{u}(q) \not{\epsilon}(\not{q} + \not{k}) \gamma^- u(p) t^a [V(q_t + k_t) - (2\pi)^2 \delta^2(q_t + k_t)] \\
M_2 &= ig \frac{1}{2p \cdot k} \bar{u}(q) \gamma^- (\not{p} - \not{k}) \not{\epsilon} u(p) [V(q_t + k_t) - (2\pi)^2 \delta^2(q_t + k_t)] t^a \\
M_3 &= ig \frac{k^-}{p \cdot q} \bar{u}(q) \gamma_\nu u(p) d^{\nu\mu}(p - q) \epsilon_\mu(k) t^b [U^{ba}(q_t + k_t) - \delta^{ba} (2\pi)^2 \delta^2(q_t + k_t)] \\
M_4 &= ig \frac{k^-}{p^-} \int \frac{d^2 l_t}{(2\pi)^2} \bar{u}(q) \gamma^- (\not{p} - \not{l}) \gamma_\nu u(p) \frac{d^{\nu\mu}(l)}{l_t^2} \epsilon_\mu(k) \\
&\quad [V(q_t + l_t) - (2\pi)^2 \delta^2(q_t + l_t)] t^b [U^{ba}(k_t - l_t) - \delta^{ba} (2\pi)^2 \delta^2(k_t - l_t)] , \quad (1)
\end{aligned}$$

where $p(q)$ is the momentum of the incoming (outgoing) quark and $z \equiv q^-/p^-$ the fractional light-cone momentum carried by the quark in the final state ($\xi \equiv 1 - z = k^-/p^-$ is that of the gluon). All other possible diagrams are suppressed by powers of energy and will be

ignored.

$$V(x_t) \equiv \hat{P} \exp \left(ig \int dz^- A_a^+(x_t, z^-) t_a \right) , \quad (2)$$

$$U(x_t) \equiv \hat{P} \exp \left(ig \int dz^- A_a^+(x_t, z^-) T_a \right) \quad (3)$$

are Wilson lines, in the fundamental and adjoint representations, respectively, running along the light cone and summing up the non-Abelian phases of the colored particles propagating through the color-field of the nucleus. To calculate the gluon production cross section, we square the sum of the amplitudes (1) and then integrate over the momentum of the outgoing quark, q_t .

After squaring the amplitude in eq. (1), it can be shown [24] that some of the terms exhibit a collinear singularity upon integration over the transverse momentum q_t of the final state quark, which arises when the quark and gluon in the final state are collinear¹. Specifically, the terms $|M_1|^2$ and $|M_3|^2$ are singular while the rest are finite. These two, unlike for example $|M_4|^2$, involve only two-point functions of Wilson lines. To leading logarithmic accuracy one can ignore the diagrams giving finite terms and keep only the contributions of diagrams which are singular, given by

$$\begin{aligned} |M_1|^2 &= 16 (p^-)^2 \frac{z(1+z^2)}{[(1-z)q_t - zk_t]^2} \int d^2 r_t e^{i(q_t+k_t)\cdot r_t} H_F(r_t) \\ |M_3|^2 &= 16 (p^-)^2 \frac{z(1+z^2)}{q_t^2} \int d^2 r_t e^{i(q_t+k_t)\cdot r_t} H_A(r_t) \end{aligned} \quad (4)$$

with

$$\begin{aligned} H_F(r_t) &\equiv C_F \int d^2 b \text{Tr}_c \langle [V^\dagger(b - r_t/2) - 1] [V(b + r_t/2) - 1] \rangle , \\ H_A(r_t) &\equiv \frac{1}{2} \int d^2 b \text{Tr}_c \langle [U^\dagger(b - r_t/2) - 1] [U(b + r_t/2) - 1] \rangle , \end{aligned} \quad (5)$$

where Tr_c denotes the trace over color matrices.

Integrating over the quark transverse momentum q_t , including the phase space factors and averaging (summing) over initial (final) state degrees of freedom leads to

$$\xi \frac{d\sigma^{qA \rightarrow gX}}{d\xi d^2 k_t} = \frac{1}{(2\pi)^2} \xi P_{g/q}(\xi) \frac{\alpha_s}{2\pi} \log \frac{Q^2}{\Lambda^2} \int d^2 r_t e^{ik_t \cdot r_t} \left[H_F(\xi r_t) + H_A(r_t) \right] \quad (6)$$

where Q^2 denotes the factorization scale. In (6) we have introduced the Leading Order (LO) quark-gluon splitting function [25]

$$\xi P_{g/q}(\xi) \equiv C_F \left[1 + (1 - \xi)^2 \right] . \quad (7)$$

It is easy to understand the origin of the two terms in (6); the first term from Fig. 1-1 corresponds to QED-like bremsstrahlung, where a free collinear gluon is emitted after

¹Care should be taken not to confuse collinear and soft singularities.

the quark scatters (multiply) from the target. This contribution vanishes in the recoilless approximation, i.e. for $z = 1 - \xi \rightarrow 1$, and has been neglected in previous computations of gluon production in the color glass condensate approach [11, 12, 13]. As we shall show, it is important when $z \sim \xi$, i.e. for production of gluons with large rapidity or Feynman- x .

The second term, from Fig. 1-3, corresponds to the case when the incoming quark radiates a collinear gluon which in turn scatters (multiply) from the target. This is the only surviving contribution for soft radiation, $\xi \rightarrow 0$, inherent in the recoilless approximation. The effect of recoil for this term is to simply replace the $\xi \rightarrow 0$ limit of the LO splitting function $P_{g/q}$ by its exact form given in (7), as expected. This leads to a suppression of high-energy (forward) radiation by a factor of 2.

To assess the QED-like contribution $\sim H_F$ from a different perspective, note that the invariant mass of the intermediate quark propagator in that diagram (see Fig. 1) is given by

$$m^2 = k_t^2 \frac{z}{\xi} + q_t^2 \frac{\xi}{z} - 2q_t \cdot k_t. \quad (8)$$

This diverges for gluons in the central rapidity region, $\xi \rightarrow 0$, and with fixed k_t , but this diagram vanishes anyways in that limit. On the other hand, for $\xi \simeq z$ we have $m^2 \simeq (k_t - q_t)^2$, which is not proportional to energy and becomes small when k_t is nearly collinear to q_t ; this kinematic configuration then gives a contribution that is not suppressed by powers of energy. The case $\xi \gg z$, finally, corresponds to “inverse Compton scattering” kinematics: a high-energy quark scatters from one or more small- x gluons and emits a high-energy gluon which takes over most of the light-cone momentum of the incident quark [26]. In order that m^2 not be large (proportional to energy), the quark has to remain nearly collinear to the beam: $q_t \lesssim \sqrt{z/\xi} q^-$. For collinear gluons with $k_t \sim \xi q_t/z \sim \sqrt{\xi/z} q^-$ then, $m^2 \simeq 0$.

The collinear logarithm in the first term of (6) can be understood as part of the one loop correction to the fragmentation function of the scattered quark while the collinear logarithm in the second term corresponds to part of the one loop correction to the gluon distribution function. To proceed further, we note that there are pieces in (6) which contribute only when the produced gluon has zero transverse momentum. Since we are interested in gluons with finite transverse momentum, those pieces can be discarded by defining fundamental and adjoint dipole cross sections at impact parameter b as follows

$$\begin{aligned} N_F(r_t, b) &\equiv \frac{1}{N_c} \text{Tr}_c \langle V^\dagger(b - r_t/2) V(b + r_t/2) - 1 \rangle \\ N_A(r_t, b) &\equiv \frac{1}{N_c^2 - 1} \text{Tr}_c \langle U^\dagger(b - r_t/2) U(b + r_t/2) - 1 \rangle \end{aligned} \quad (9)$$

in terms of which the cross section (6) can be rewritten as

$$\xi \frac{d\sigma^{qA \rightarrow gX}}{d\xi d^2k_t d^2b} = \frac{1}{(2\pi)^2} \xi P_{g/q}(\xi) \frac{\alpha_s}{2\pi} \log \frac{Q^2}{\Lambda^2} \left[\frac{1}{\xi^2} N_F(k_t/\xi, b) + N_A(k_t, b) \right]. \quad (10)$$

So far, we have calculated the gluon production cross section from scattering of quarks on the target nucleus. Before we can relate this to hadron production in proton-nucleus collisions, we need to include all other processes, to the same order in α_s , which contribute to hadron production. These are, for example, elastic and inelastic production of quarks as well as production of gluons from scattering of gluons on the target nucleus². Details will be reported elsewhere [24]. Nevertheless, the final result is quite simple and can be written down in analogy to eq. (10):

$$\xi \frac{d\sigma^{qA \rightarrow qX}}{d\xi d^2k_t d^2b} = \frac{1}{(2\pi)^2} \xi P_{g/q}(\xi) \frac{\alpha_s}{2\pi} \log \frac{Q^2}{\Lambda^2} \left[N_A(k_t, b) + \frac{1}{\xi^2} N_F(k_t/\xi, b) \right] \quad (11)$$

$$\xi \frac{d\sigma^{qA \rightarrow qX}}{d\xi d^2k_t d^2b} = \frac{1}{(2\pi)^2} \xi P_{q/q}(\xi) \frac{\alpha_s}{2\pi} \log \frac{Q^2}{\Lambda^2} \left[N_F(k_t, b) + \frac{1}{\xi^2} N_F(k_t/\xi, b) \right] \quad (12)$$

$$\xi \frac{d\sigma^{gA \rightarrow qX}}{d\xi d^2k_t d^2b} = \frac{1}{(2\pi)^2} \xi P_{q/g}(\xi) \frac{\alpha_s}{2\pi} \log \frac{Q^2}{\Lambda^2} \left[N_F(k_t, b) + \frac{1}{\xi^2} N_A(k_t/\xi, b) \right] \quad (13)$$

$$\xi \frac{d\sigma^{gA \rightarrow gX}}{d\xi d^2k_t d^2b} = \frac{1}{(2\pi)^2} \xi P_{g/g}(\xi) \frac{\alpha_s}{2\pi} \log \frac{Q^2}{\Lambda^2} \left[N_A(k_t, b) + \frac{1}{\xi^2} N_A(k_t/\xi, b) \right] \quad (14)$$

with the LO splitting functions as given in [25]. Contributions of processes involving anti-quarks are identical to those from quarks to this order. Here, we denote the momentum fraction of the produced daughter parton by ξ , and its transverse momentum by k_t . For completeness, we also need to include the elastic scattering contributions to quark and gluon production [3] given by

$$\xi \frac{d\sigma^{qA \rightarrow qX}}{d\xi d^2k_t d^2b} = \frac{2}{(2\pi)^2} \xi \delta(1 - \xi) N_F(k_t, b) \quad (15)$$

$$\xi \frac{d\sigma^{gA \rightarrow gX}}{d\xi d^2k_t d^2b} = \frac{2}{(2\pi)^2} \xi \delta(1 - \xi) N_A(k_t, b) \quad (16)$$

We now reorganize the different pieces from eqs. (11 - 16) in a way which makes the connection to the DGLAP evolution of parton distribution and fragmentation functions obvious. We consider the diagrams corresponding to the DGLAP evolution of quark distribution functions first. They are given by (half of) eq. (15) and the first terms of (12) and (13). Multiplying by the bare (parton model) quark and gluon distribution functions $q_0(x/\xi)$, $g_0(x/\xi)$ we obtain

$$\int_x^1 \frac{d\xi}{\xi} \left\{ q_0\left(\frac{x}{\xi}\right) \left(\delta(1 - \xi) + \frac{\alpha_s}{2\pi} \log \frac{Q^2}{\Lambda^2} P_{q/q}(\xi) \right) + g_0\left(\frac{x}{\xi}\right) \frac{\alpha_s}{2\pi} \log \frac{Q^2}{\Lambda^2} P_{q/g}(\xi) \right\} N_F(\xi, k_t, b) \\ \rightarrow f_{q/p}(x/\xi, Q^2) \otimes N_F(\xi, k_t, b) \quad (17)$$

where $f_{q/p}(x, Q^2)$ is the renormalized (DGLAP evolved) quark distribution function in a proton. We have used the DGLAP evolution equation for the quark distribution function.

²The diagrams considered here correspond to real corrections, one needs to include the virtual corrections to get the full splitting function.

Next, consider evolution of the gluon distribution function. The relevant terms are given by (half of) eq. (16), and the first terms of (11) and (14). Putting them together we obtain

$$\int_x^1 \frac{d\xi}{\xi} \left\{ g_0\left(\frac{x}{\xi}\right) \left[\delta(1-\xi) + \frac{\alpha_s}{2\pi} \log \frac{Q^2}{\Lambda^2} P_{g/g}(\xi) \right] + q_0\left(\frac{x}{\xi}\right) \frac{\alpha_s}{2\pi} \log \frac{Q^2}{\Lambda^2} P_{g/q}(\xi) \right\} N_A(\xi, k_t, b) \\ \rightarrow f_{g/p}(x/\xi, Q^2) \otimes N_A(\xi, k_t, b) \quad (18)$$

where $f_{g/p}(x, Q^2)$ is the renormalized (DGLAP evolved) gluon distribution function in a proton.

The remaining diagrams lead to DGLAP evolution of the fragmentation functions. We start with the quark fragmentation function given by (half of) eq. (15) and the second terms in eqs. (11-12)

$$\int_x^1 \frac{d\xi}{\xi} \left[D_q^0\left(\frac{x}{\xi}\right) \left(\delta(1-\xi) + \frac{\alpha_s}{2\pi} \log \frac{Q^2}{\Lambda^2} P_{q/q}(\xi) \right) + D_g^0\left(\frac{x}{\xi}\right) \frac{\alpha_s}{2\pi} \log \frac{Q^2}{\Lambda^2} P_{g/q}(\xi) \right] \widetilde{N}_F(\xi, k_t, b) \\ \rightarrow D_q(x/\xi, Q^2) \otimes \widetilde{N}_F(\xi, k_t, b) \quad (19)$$

where $D_q(x, Q^2)$ is the DGLAP evolved quark-hadron fragmentation function and $\widetilde{N}_F(\xi, k_t, b) \equiv N_F(\xi, k_t/\xi, b)/\xi^2$. The rest of the diagrams give

$$\int_x^1 \frac{d\xi}{\xi} \left[D_g^0\left(\frac{x}{\xi}\right) \left(\delta(1-\xi) + \frac{\alpha_s}{2\pi} \log \frac{Q^2}{\Lambda^2} P_{g/g}(\xi) \right) + D_q^0\left(\frac{x}{\xi}\right) \frac{\alpha_s}{2\pi} \log \frac{Q^2}{\Lambda^2} P_{q/g}(\xi) \right] \widetilde{N}_A(\xi, k_t, b) \\ \rightarrow D_g(x/\xi, Q^2) \otimes \widetilde{N}_A(\xi, k_t, b) \quad (20)$$

where $\widetilde{N}_A(\xi, k_t, b) \equiv N_A(\xi, k_t/\xi, b)/\xi^2$. The final result for one parton radiation can be schematically summarized as the following

$$\rightarrow f_q(Q^2) \otimes N_F \otimes D_0^q + q_0 \otimes \widetilde{N}_F \otimes D_q(Q^2) + f_g(Q^2) \otimes N_A \otimes D_0^g + g_0 \otimes \widetilde{N}_A \otimes D_g(Q^2) \quad (21)$$

where $f_{q,g}(Q^2)$, $D_{q,g}(Q^2)$ correspond to DGLAP evolved quark and gluon distribution and fragmentation functions, respectively; f_0 , D_0 are the bare distribution and fragmentation functions, and \otimes denotes a convolution in x (not shown explicitly).

The expression (21) is, however, not the complete result as should be clear from the presence of bare (non-DGLAP evolved) distribution and fragmentation functions. To get the complete one loop result, one needs to consider one additional parton radiation. For example, for the diagram shown in Fig. 1-1, one needs to allow for gluon radiation from the initial quark line also, which contributes to the one-loop DGLAP evolution of the bare quark distribution function. This contribution is calculated in appendix A. The full calculation will be shown elsewhere [24], here we just quote the final result for hadron production in proton-nucleus collisions

$$\frac{d\sigma^{pA \rightarrow hX}}{dY d^2P_t d^2b} = \frac{1}{(2\pi)^2} \int_{x_F}^1 dx \frac{x}{x_F} \left\{ f_{q/p}(x, Q^2) N_F\left[\frac{x}{x_F} P_t, b\right] D_{h/q}\left(\frac{x_F}{x}, Q^2\right) + \right. \\ \left. f_{g/p}(x, Q^2) N_A\left[\frac{x}{x_F} P_t, b\right] D_{g/h}\left(\frac{x_F}{x}, Q^2\right) \right\} \quad (22)$$

where Y and P_t are the rapidity and transverse momentum of the produced hadron while x_F denotes its Feynman- x . Eq. (22) is our main result. It should be noted that all additional parton radiations are taken into account by using the solution of the DGLAP evolution equations for the quark and gluon distribution and fragmentation functions.

3 Forward hadron production in dA collisions at RHIC

We now apply our results to deuteron-gold collisions at RHIC. We use the Leading Order CTEQ5 distribution functions for a proton [27] with $Q^2 = P_t^2$, employing isospin symmetry to obtain those of the neutron, and the LO KKP fragmentation functions [28] into charged hadrons (divided by two). For a deuteron projectile, the difference to fragmentation into negatively charged hadrons is small and nearly independent of transverse momentum.

For our numerical results shown below, we employ the following parameterization³ for the dipole cross section from ref. [6]:

$$N_A(r_t, y) = \exp \left[-\frac{1}{4} [r_t^2 Q_s^2(y)]^{\gamma(y, k_t)} \right] - 1 . \quad (23)$$

Here,

$$Q_s(y) = Q_0 \exp[\lambda(y - y_0)/2] , \quad (24)$$

is the saturation momentum of the nucleus at the rapidity y of the produced parton, which can be obtained from its longitudinal momentum x and its transverse momentum $k_t = xP_t/x_F$. The reference point $y_0 = 0.6$ specifies where effects due to quantum evolution start to become important. Q_0 is the initial condition for the saturation momentum at y_0 , and the growth rate $\lambda \approx 0.3$.

Since data for central collisions is not publicly available yet, we focus on minimum-bias collisions. We take an average saturation momentum near midrapidity of $Q_0 = 1$ GeV [6]. The scattering amplitude for a dipole in the fundamental representation, N_F , can also be parameterized as in (23), with the replacement $Q_s^2 \rightarrow Q_s^2 C_F/C_A = \frac{4}{9} Q_s^2$.

In (23), $\gamma(y, k_t)$ denotes the anomalous dimension with saturation boundary condition. Ref. [6] employed the following model for the anomalous dimension which reduces to the DGLAP anomalous dimension ($=1$) in the high transverse momentum limit:

$$\gamma(y, k_t) = \frac{1}{2} \left(1 + \frac{|\xi(y, k_t)|}{|\xi(y, k_t)| + \sqrt{2}|\xi(y, k_t)| + 28\zeta(3)} \right) , \quad (25)$$

where

$$\xi(y, k_t) = \frac{\log(k_t^2/Q_0^2)}{(\lambda/2)(y - y_0)} . \quad (26)$$

³Our convention for the sign is opposite to that of ref. [6], which is due to the definitions (9).

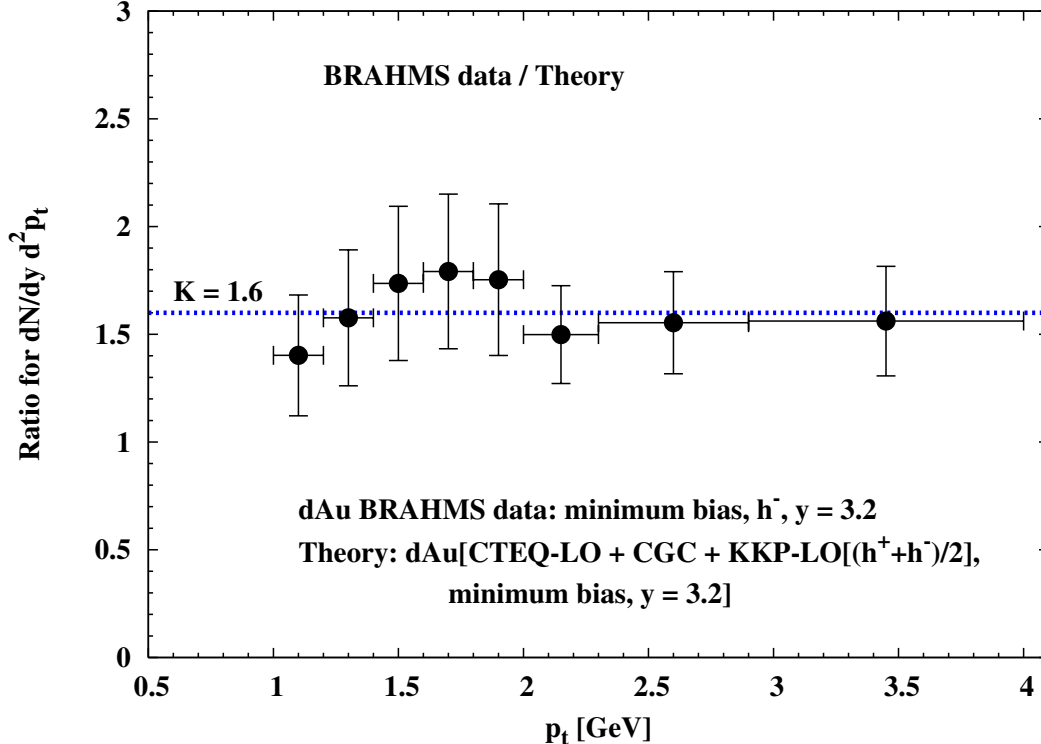


Figure 2: P_t dependence of our results compared to BRAHMS minimum bias data.

This function vanishes for fixed k_t and $y \rightarrow \infty$, and so $\gamma \rightarrow 1/2$. On the other hand, near the boundary to the quantum evolution regime (i.e. at small rapidity $y \simeq y_0$ such that $Q_s \simeq Q_0$) the anomalous dimension $\gamma \rightarrow 1$, as appropriate for the classical McLerran-Venugopalan (MV) model [29]. For both $\gamma = 1/2$ and $\gamma = 1$ the Fourier transform of $N_A(r_t)$ can be performed analytically:

$$N_A^{\gamma=1}(k_t^2) = \int d^2 r_t e^{ik_t \cdot r_t} N_A^{\gamma=1}(r_t) = \frac{4\pi}{Q_s^2} \exp(-k_t^2/Q_s^2), \quad (27)$$

$$N_A^{\gamma=1/2}(k_t^2) = \int d^2 r_t e^{ik_t \cdot r_t} N_A^{\gamma=1/2}(r_t) = \frac{32\pi}{Q_s^2} \frac{1}{(1 + 16 k_t^2/Q_s^2)^{3/2}}. \quad (28)$$

Hence, there is an exponential drop with k_t^2 for the MV model [30] with $\gamma = 1$, and a power-law decrease if the anomalous dimension $\gamma = 1/2$. Therefore, we expect a steeper P_t -distribution of hadrons for the classical MV model. In the general case, when γ depends on k_t and y , the Fourier transform has to be done numerically.

In Fig. 2, we show the transverse momentum dependence of the h^- data by BRAHMS [31] relative to our results, on a linear scale. The transverse momentum dependence of the data is reproduced very well. For the correct absolute normalization, we need to multiply by a K -factor of about 1.6; this is not surprising since our calculation has been performed at Leading Order (in α_s). In fact, from our point of view it is rather comforting that there is room for the expected large NLO corrections.

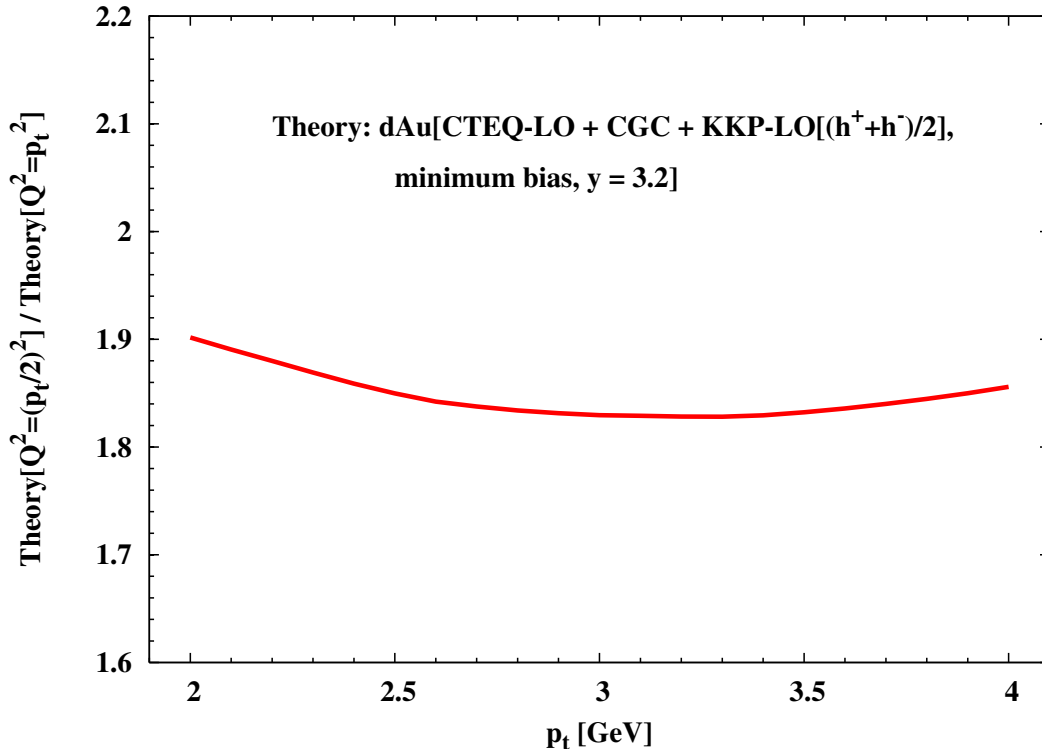


Figure 3: Ratio of the transverse momentum distributions of charged hadrons for $Q^2 = (P_t/2)^2$ and $Q^2 = P_t^2$.

To test the scale dependence of our LO result, we plot the ratio of the distributions for $Q^2/P_t^2 = 1$ and $Q^2/P_t^2 = 1/4$ in Fig. 3. For LO computations there is, in general, a monotonic dependence on the hard scale and so “optimal scales” [32], where the result is stable against small variations of Q^2/P_t^2 , can not be defined. Nevertheless, we observe that for $Q^2/P_t^2 = 1/4$ [32] the shape of the distribution does turn out to be nearly the same as for $Q^2/P_t^2 = 1$, and that the overall K -factor drops to ~ 1 . This indicates that NLO corrections should not change the shape of the distribution by much. In what follows, we return to the generic scale $Q^2 = P_t^2$ and fix $K = 1.6$.

Next, we consider the relative contributions of quarks and gluons in Fig. 4. At rapidity ~ 3 and $p_t \geq 1$ GeV quarks clearly dominate [3]. This, of course, is an essential difference to the central rapidity region, where gluons contribute more. At yet larger rapidity quarks would dominate even at lower p_t , and their independent fragmentation should lead to a downward shift of baryon-number, which is initially concentrated about beam rapidity [33].

In Fig. 5, we compare the full calculation with DGLAP evolution of the distribution and fragmentation functions to one where Q^2 has been fixed to 1 GeV^2 . It is obvious that DGLAP evolution is important and that it improves the agreement with the data significantly. Physically, this is because collinear parton radiation shifts the hard partons to smaller momentum fractions, which is the above-mentioned recoil effect, and softens the p_t -distribution of produced hadrons. The effect is clearly seen in the data. This emphasizes

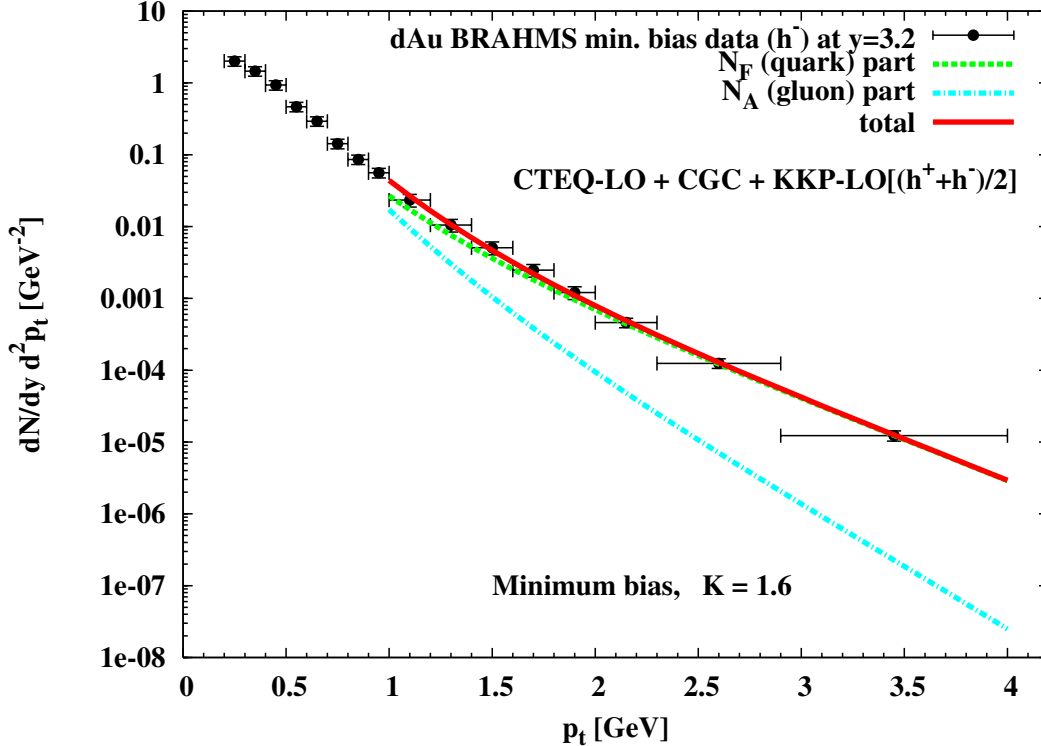


Figure 4: Relative contribution of quarks and gluons from the projectile deuteron.

that full splitting functions, rather than their soft recoilless limit, have to be employed for hadron production in the forward region.

We also show the result of a calculation within the classical McLerran-Venugopalan model, which assumes that the anomalous dimension $\gamma = 1$. The resulting distribution of hadrons is much too soft. It is clear that the data requires the proper quantum evolution of the target density, with an anomalous dimension γ close to $1/2$ (with only a weak dependence on transverse momentum). This feature is shared by the KKT [6] and IIM [34] dipole models, both of which provide a good description of the BRAHMS data.

Fig. 6 shows the π^0 distribution in minimum-bias $d + Au$ collisions at rapidity $y = 4$, which is currently investigated by STAR. Here, x -evolution leads to an increase of the saturation momentum by $\sim 13\%$ as compared to the BRAHMS kinematics. The projectile partons need to carry yet larger momentum fractions (and fragment into faster hadrons), hence Q^2 -evolution due to emissions has an even stronger “softening” effect on the final hadronic spectra (roughly one order of magnitude at $p_t = 3$ GeV). The P_t -distribution at $y = 4$ is close to exponential for $P_t : 1 \rightarrow 2.5$ GeV. At higher transverse momentum the convex behavior of the projectile parton distribution and fragmentation functions eventually takes over. However, due to the very steep distribution the relative deviation of the classical MV model from the full result including quantum evolution in x is smaller than for the BRAHMS kinematics. Forthcoming STAR data will test this prediction (for preliminary data at intermediate P_t see [35]).

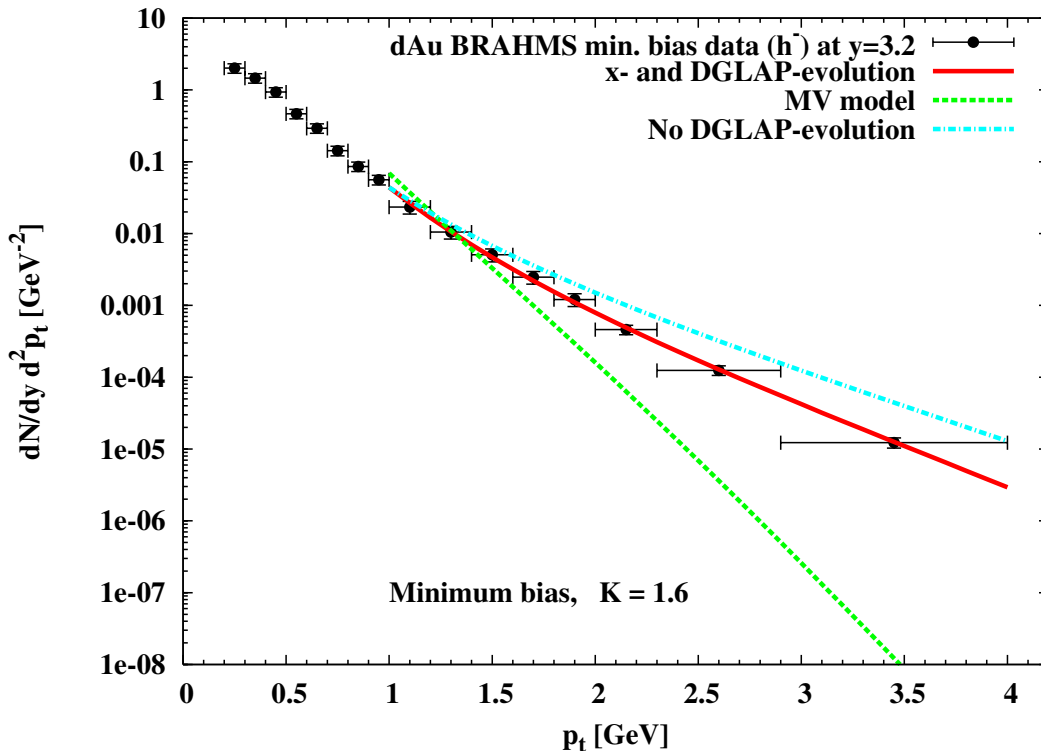


Figure 5: Importance of DGLAP evolution of the proton/hadron distribution/fragmentation functions and of the anomalous dimension of the target gluon distribution.

4 Summary

In summary, we have shown that high-energy proton-nucleus collisions can be described as scattering of collinearly factorized partons (which evolve according to the DGLAP equation) in the proton on a dense nucleus treated as a Color Glass Condensate. We have isolated diagrams with collinear singularities which lead to logarithms of Q^2 and proven that they satisfy DGLAP evolution. Only two-point functions of Wilson lines, i.e. dipoles, contribute to the single-inclusive cross-section; in the future, these could be obtained from the JIMWLK small- x evolution equation.

To apply our results to data from RHIC, we have presently adopted a phenomenological dipole parametrization due to Kharzeev, Kovchegov and Tuchin. The minimum-bias data from $d + Au$ collisions at forward rapidity obtained by the BRAHMS collaboration can be reproduced very well with a transverse momentum *independent* K -factor of 1.6 (for $Q^2 = P_t^2$). Hence, NLO corrections are expected to be large but should not distort the shape of the transverse momentum distributions obtained from our LO analysis.

We have shown that in order to reproduce the shape of the measured transverse momentum distribution, one needs to account for both Q^2 -evolution of the projectile parton distribution functions and of the fragmentation functions, as well as for quantum evolution

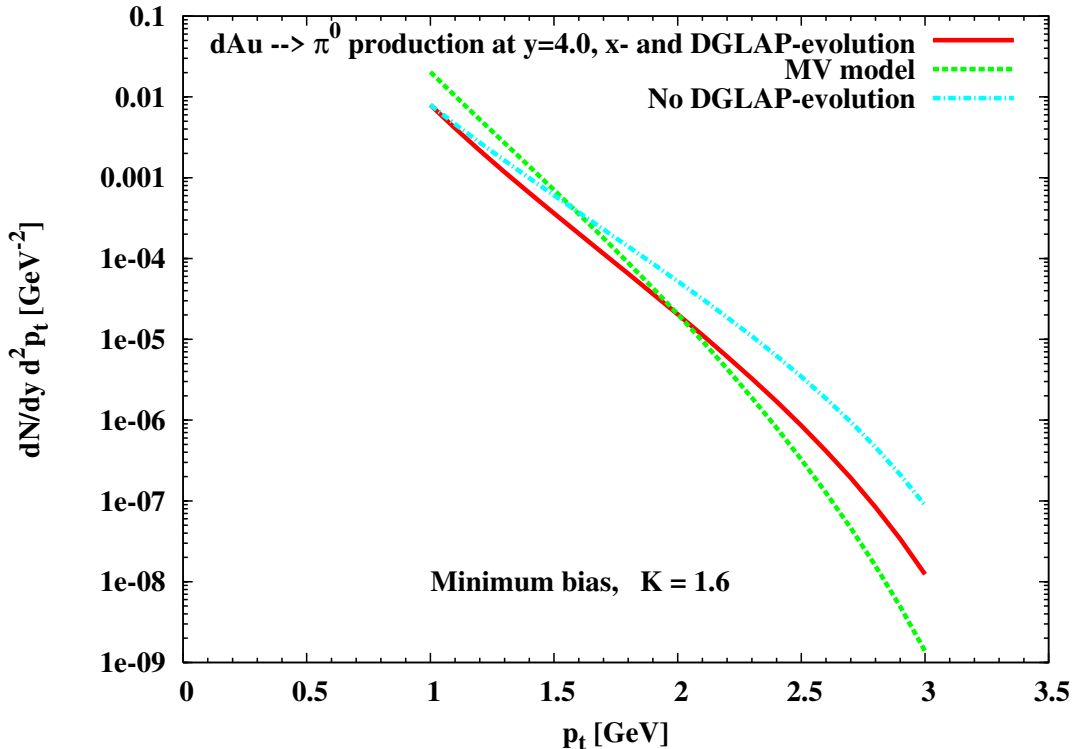


Figure 6: Same as Fig. 5 but for π^0 production at rapidity $y = 4$.

of the small- x field of the target nucleus. Neglect of “recoil” effects from DGLAP evolution leads to a significantly harder p_t distribution than the data; a purely classical target field with anomalous dimension $\gamma = 1$ produces a much softer distribution. The fact that both of these key components, and of their interplay, is seen in the data represents important evidence for the Color Glass Condensate from RHIC.

In the future, it would be useful if *central* rather than minimum-bias data were available. For central collisions the saturation momentum of the nucleus increases by $\sim 50\%$ and so the saturation regime extends to higher transverse momentum. Also, it will be interesting to see whether forthcoming data from STAR for π^0 production at yet larger rapidity, $y \sim 4$, can be reproduced equally well; we have provided a prediction based on the current setup. A better p_t -resolution will be important to constrain the dipole profiles more tightly. Quantitative theoretical ab-initio computations of those universal CGC functions will hopefully emerge in the near future. We have provided a systematical framework which will make it possible to compare them to experimental data.

Acknowledgments

We would like to thank L. Frankfurt, F. Gelis, M. Strikman and W. Vogelsang for useful discussions. J.J-M. is supported in part by the U.S. Department of Energy under Grant No. DE-FG02-00ER41132.

A Radiation from both initial and final state

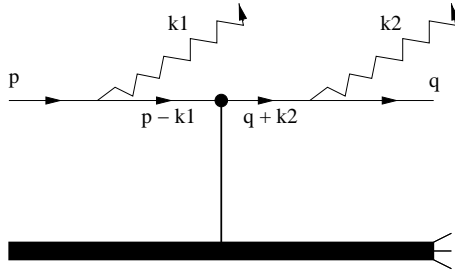


Figure 7: One of the diagrams contributing to DGLAP evolution of bare quark distribution and fragmentation functions.

The diagram considered here is shown in Fig. 7. The cross section for this process is

$$q^- \frac{d\sigma^{qA \rightarrow qX}}{dq^- d^2 q_t d^2 b} = \frac{1}{2p^-} \frac{1}{2(2\pi)^3} \int \frac{d^3 k_1}{(2\pi)^3 2k_1^-} \int \frac{d^3 k_2}{(2\pi)^3 2k_2^-} |M|^2 \quad (29)$$

which can be related to hadron production cross section via

$$P_h^- \frac{d\sigma^{pA \rightarrow hX}}{dP_h^- d^2 P_t d^2 b} \equiv \int dx_q q_0(x_q) \int dz_h D_0(z_h) q^- \frac{d\sigma^{qA \rightarrow qX}}{dq^- d^2 q_t d^2 b} . \quad (30)$$

We have defined $x_q = p^-/P^-$, $z_h = P_h^-/q^-$ and p^- , P^- are the momenta of the incoming quark and proton respectively, while q^- , P_h^- are the momenta of the outgoing quark and hadron. We also define $z_1 = (p^- - k_1^-)/p^-$ and $z_2 = q^-/(q^- + k_2^-)$. The matrix element is given by

$$M^{\mu\nu} = g^2 \bar{u}(q) \gamma^\nu t^b S_F^0(q + k_2) \tau_f(q + k_2, p - k_1) S_F^0(p - k_1) \gamma^\mu t^a u(p) , \quad (31)$$

where

$$\tau_f(q, p) \equiv (2\pi) \delta(p^- - q^-) \gamma^- \int d^2 x e^{i(q_t - p_t) \cdot x_t} [V(x_t) - 1] . \quad (32)$$

We need to contract this with the polarization vectors for the two radiated gluons $\epsilon_\mu(k_1, \lambda_1)$, $\epsilon_\nu(k_2, \lambda_2)$ and then square it. Using the polarization tensor $\sum_\lambda \epsilon_\mu^*(k, \lambda) \epsilon_\nu(k, \lambda) \equiv$

$[-g_{\mu\nu} + \frac{\eta_\mu k_\nu + \eta_\nu k_\mu}{\eta \cdot k}]$, we get

$$\begin{aligned}
|M|^2 &= \frac{g^4}{2} \frac{1}{(q+k_2)^4} \frac{1}{(p-k_1)^4} [-g_{\mu\delta} + \frac{\eta_\mu k_{1\delta} + \eta_\delta k_{1\mu}}{\eta \cdot k_1}] [-g_{\nu\rho} + \frac{\eta_\nu k_{2\rho} + \eta_\rho k_{2\nu}}{\eta \cdot k_2}] \\
&\quad Tr_D \left[\not{h} \gamma^\nu (\not{h} + k_2) \gamma^- (\not{p} - k_1) \gamma^\mu \not{p} \gamma^\delta (\not{p} - k_1) \gamma^- (\not{h} + k_2) \gamma^\rho \right] \\
&\quad Tr_c \left[t^{btb} [V(q_t + k_{2t} + k_{1t} - p_t) - (2\pi)^2 \delta^2(q_t + k_{2t} + k_{1t} - p_t)] \right. \\
&\quad \left. t^{at^a} [V^\dagger(q_t + k_{2t} + k_{1t} - p_t) - (2\pi)^2 \delta^2(q_t + k_{2t} + k_{1t} - p_t)] \right] \quad (33)
\end{aligned}$$

where Tr_D, Tr_c stand for traces over spinor and color matrices. Evaluating the trace of the spinors above is algebraically involved but straightforward. Contracted with the gluon polarization tensors, it is given by

$$[-g_{\mu\delta} + \dots] [-g_{\nu\rho} + \dots] Tr_D[\dots] = 124 p^- q^- (p \cdot k_1) (q \cdot k_2) \frac{(1+z_1)(1+z_2)}{z_2(1-z_1)(1-z_2)} \quad (34)$$

where z_1, z_2 are defined above. Putting everything together, the partonic cross section can be written as

$$\begin{aligned}
q^- \frac{d\sigma^{qA \rightarrow qX}}{dq^- d^2q_t d^2b} &= \frac{g^4 C_F^2}{(2\pi)^4} q^- P^- \int \frac{dz_1}{z_1} \frac{1+z_1^2}{1-z_1} \int \frac{dz_2}{z_2^3} \frac{1+z_2^2}{1-z_2} \delta(x_q - \frac{q^-}{z_1 z_2 P^-}) \int d^2x_t d^2y_t \\
&\quad e^{iq_t \cdot (x_t - y_t)} \int \frac{d^2k_{1t}}{(2\pi)^2} \frac{e^{ik_{1t} \cdot (x_t - y_t)}}{k_{1t}^2} \int \frac{d^2k_{2t}}{(2\pi)^2} \frac{e^{ik_{2t} \cdot (x_t - y_t)}}{[k_{2t} - \frac{1-z_2}{z_2} q_t]^2} Tr_c \left[[V(x_t) - 1] [V^\dagger(y_t) - 1] \right] \quad (35)
\end{aligned}$$

Again, the integrations over the transverse momenta k_{1t}, k_{2t} exhibit collinear singularities which lead to logarithms of Q^2 , so that the cross section can be written as

$$\begin{aligned}
q^- \frac{d\sigma^{qA \rightarrow qX}}{dq^- d^2q_t d^2b} &= \frac{1}{(2\pi)^2} \frac{q^-}{P^-} \int \frac{dz_1}{z_1} \left[\frac{\alpha_s}{2\pi} \ln \frac{Q^2}{\Lambda^2} C_F \frac{1+z_1^2}{1-z_1} \right] \int \frac{dz_2}{z_2^3} \left[\frac{\alpha_s}{2\pi} \ln \frac{Q^2}{\Lambda^2} C_F \frac{1+z_2^2}{1-z_2} \right] \\
&\quad \delta(x_q - \frac{q^-}{z_1 z_2 P^-}) N_F[\frac{q_t}{z_2}, b] \quad (36)
\end{aligned}$$

Using (36) in (30) and combining it with the relevant term in (21) gives the quark contribution to the hadronic cross section

$$\begin{aligned}
\frac{d\sigma^{pA \rightarrow hX}}{dy d^2P_t d^2b} &= x_F \int \frac{dz_1}{z_1} \frac{dz_2}{z_2} \frac{dz_h}{z_h} q_0[\frac{x_F}{z_1 z_2 z_h}] \left[\delta(1-z_1) + \frac{\alpha_s}{2\pi} \ln \frac{Q^2}{\Lambda^2} P_{q/q}(z_1) \right] \\
&\quad D_0(z_h) \left[\delta(1-z_2) + \frac{\alpha_s}{2\pi} \ln \frac{Q^2}{\Lambda^2} P_{q/q}(z_2) \right] \frac{1}{(2\pi)^2} \frac{1}{(z_2 z_h)^2} N_F[\frac{P_t}{z_2 z_h}, b] \quad (37)
\end{aligned}$$

Defining the DGLAP evolved quark distribution function $f_q(\frac{x_F}{z_2 z_h}, Q^2)$ as

$$f_q(\frac{x_F}{z_2 z_h}, Q^2) \equiv \int \frac{dz_1}{z_1} q_0(\frac{x_F}{z_1 z_2 z_h}) \left[\delta(1-z_1) + \frac{\alpha_s}{2\pi} \ln \frac{Q^2}{\Lambda^2} P_{q/q}(z_1) \right], \quad (38)$$

then changing variables to $z'_h \equiv z_2 z_h$, and defining the DGLAP evolved fragmentation function $D_q(z'_h, Q^2)$ as

$$D_q(z'_h, Q^2) \equiv \int \frac{dz_2}{z_2} D_0\left(\frac{z'_h}{z_2}\right) \left[\delta(1 - z_2) + \frac{\alpha_s}{2\pi} \ln \frac{Q^2}{\Lambda^2} P_{q/q}(z_2) \right] \quad (39)$$

leads to the DGLAP evolved hadron production cross section

$$\frac{d\sigma^{pA \rightarrow hX}}{dy d^2P_t d^2b} = \int_{x_F}^1 dz'_h \frac{x_F}{z'_h} f_q\left(\frac{x_F}{z'_h}, Q^2\right) D_q(z'_h, Q^2) \frac{1}{(2\pi)^2} \frac{1}{z_h'^2} N_F\left[\frac{P_t}{z'_h}, b\right]. \quad (40)$$

It should be noted that one also needs to include diagrams where one integrates over the final state quark momenta rather than the gluon momenta as we have done here. This would bring in the quark-gluon splitting function $P_{g/q}$ which, combined with $P_{q/q}$ above, would then go into the DGLAP evolution of the quark distribution or fragmentation function in (38, 39). A further change of variables $x = x_F/z'_h$ in (40) then gives the first part of (22). Contribution of the diagrams involving an incoming gluon are similar and give the second part of (22).

B $2 \rightarrow 1$ kinematics

In this appendix we elaborate on the $2 \rightarrow 1$ like kinematics employed above. In particular, we show that energy-momentum conservation implies that much smaller momentum fractions are probed in the target than for $2 \rightarrow 2$ kinematics underlying leading-twist perturbative computations (see e.g. [8]). We work in a frame where both projectile and target have large light-cone momenta, for example the center of rapidity frame. The various momenta as used within this appendix are defined in Fig. 8. The incoming parton carries

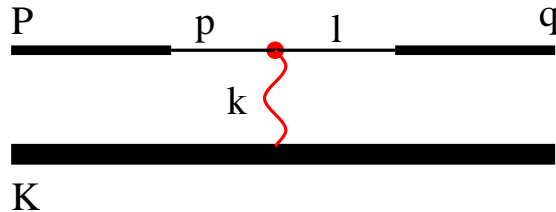


Figure 8: The $2 \rightarrow 1$ kinematics.

momentum p while that of the projectile nucleons is labeled P ; the outgoing parton's momentum is l while that of the outgoing hadron is q . The momentum of the nucleons from the incoming nucleus is K , and k is the exchange between the parton and the nucleus. More explicitly⁴,

$$P^\mu = (P^- = \sqrt{s/2}, P^+ = 0, P_t = 0)$$

⁴We follow the convention from the main text that P and q have large minus-components, i.e. that the rapidities of both the projectile and of the produced hadron are large and negative. To comply with standard practice, however, in the final figures we quote the modulus of the rapidity of the detected hadron, $y_h \equiv -Y > 0$.

$$\begin{aligned}
p^\mu &= (p^- = x P^-, p^+ = 0, p_t = 0) \\
l^\mu &= (l^- = p^-, l^+ = \frac{l_t^2}{2l^-}, l_t) \\
q^\mu &= (q^- = z l^-, q^+ = \frac{q_t^2}{2q^-}, q_t = z l_t) \\
k^\mu &= (k^- \approx 0, k^+ = x_A K^+, k_t) \\
K^\mu &= (K^- = 0, K^+ = \sqrt{s/2}, K_t = 0)
\end{aligned} \tag{41}$$

and

$$l = p + k \tag{42}$$

from energy-momentum conservation. The only approximation made in (41) is setting $k^- \approx 0$ which corresponds to the eikonal approximation. Using (42), we have $k_t = l_t$, $xP^- = l^-$ and $k^+ = l^+$, so that $z = x_F/x$ and, finally,

$$x_A = \frac{x q_t^2}{x_F^2 s}, \tag{43}$$

where Feynman- x is defined as $x_F \equiv q^-/\sqrt{s/2}$. This relation can be rewritten in terms of the rapidity of the produced hadron, Y (which in the massless limit equals that of its parent parton):

$$x_A \equiv x e^{-2y_h}. \tag{44}$$

Here, $y_h \equiv -Y > 0$ denotes the modulus of the rapidity of the observed final-state hadron. In terms of its momentum, its rapidity is given by $q^- \equiv q_t e^{y_h}/\sqrt{2}$.

Equation (43) relates x_A to the momentum fraction x carried by the impinging projectile parton, and to the transverse momentum and Feynman- x of the produced hadron. Hence, we can insert this form inside the integral from eq. (22), then divide by eq. (22) itself, to determine the average x_A probed in the target nucleus. It is clear from (43) that $\langle x_A \rangle \rightarrow q_t^2/s \sim 10^{-4}$ as $x_F \rightarrow 1$ (since $1 \geq x \geq x_F$). The result for both BRAHMS and STAR kinematics is shown in Fig. 9. It turns out that for BRAHMS kinematics for example, $\langle x_A \rangle \approx 10^{-3}$, which is more than an order of magnitude smaller than for the $2 \rightarrow 2$ kinematics employed in leading-twist calculations [8].

In Fig. 10 we show the kinematic region in x which contributes to the cross section given by (22), at hadron transverse momentum $q_t = 2$ GeV and rapidity $y_h = 3.2$ and 4, respectively. Clearly, the cross section is dominated by very large x (labeled in this figure as x_p) and very small values of x_A .

References

- [1] I. Arsene *et al.* [BRAHMS Collaboration], nucl-ex/0410020; B. B. Back *et al.*, [PHOBOS Collaboration], nucl-ex/0410022; K. Adcox *et al.* [PHENIX Collaboration], nucl-ex/0410003; J. Adams [STAR Collaboration], nucl-ex/0501009.

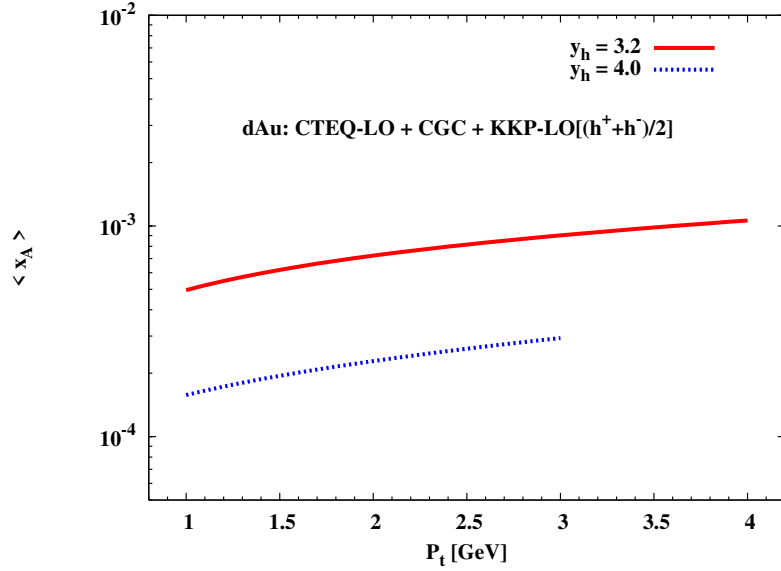


Figure 9: The average momentum fraction probed in the target for forward hadron production at RHIC energy, versus the transverse momentum of the hadron.

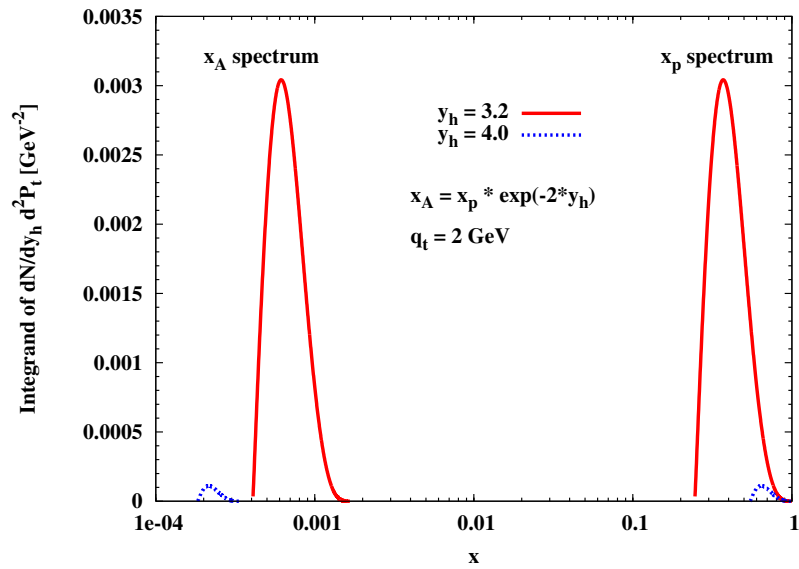


Figure 10: The momentum fractions of projectile and target partons contributing to the cross section from eq. (22).

- [2] A. H. Mueller, Nucl. Phys. A **715**, 20 (2003); E. Iancu and R. Venugopalan, hep-ph/0303204; J. Jalilian-Marian, Mod. Phys. Lett. A **19**, 1251 (2004); J. Jalilian-Marian and Y. V. Kovchegov, arXiv:hep-ph/0505052; L. McLerran, Nucl. Phys. A **752**, 355 (2005); E. Levin, J. Phys. Conf. Ser. **5**, 127 (2005) [arXiv:hep-ph/0408039].
- [3] A. Dumitru and J. Jalilian-Marian, Phys. Rev. Lett. **89**, 022301 (2002).
- [4] I. Vitev, Phys. Lett. B **562**, 36 (2003); J. Jalilian-Marian, Y. Nara and R. Venugopalan, Phys. Lett. B **577**, 54 (2003); F. Gelis and J. Jalilian-Marian, Phys. Rev. D **66**, 014021 (2002), Phys. Rev. D **66**, 094014 (2002), Phys. Rev. D **67**, 074019 (2003).
- [5] D. Kharzeev, Y. V. Kovchegov and K. Tuchin, Phys. Rev. D **68**, 094013 (2003); J. L. Albacete, N. Armesto, A. Kovner, C. A. Salgado and U. A. Wiedemann, Phys. Rev. Lett. **92**, 082001 (2004); E. Iancu, K. Itakura and D. N. Triantafyllopoulos, Nucl. Phys. A **742**, 182 (2004).
- [6] D. Kharzeev, Y. V. Kovchegov and K. Tuchin, Phys. Lett. B **599**, 23 (2004).
- [7] J. Jalilian-Marian, Nucl. Phys. A **748**, 664 (2005).
- [8] V. Guzey, M. Strikman and W. Vogelsang, Phys. Lett. B **603**, 173 (2004).
- [9] H. J. Drescher, A. Dumitru and M. Strikman, arXiv:hep-ph/0408073; arXiv:hep-ph/0501165.
- [10] R. C. Hwa, C. B. Yang and R. J. Fries, nucl-th/0410111; J. Qiu and I. Vitev, arXiv:hep-ph/0405068; B. Z. Kopeliovich, J. Nemchik, I. K. Potashnikova, M. B. Johnson and I. Schmidt, arXiv:hep-ph/0501260.
- [11] For computations of the leading-twist perturbative gluon spectrum ($k_t \gg Q_s$) see A. Kovner, L. D. McLerran and H. Weigert, Phys. Rev. D **52**, 3809 (1995); M. Gyulassy and L. D. McLerran, Phys. Rev. C **56**, 2219 (1997); Yu. V. Kovchegov and D. H. Rischke, Phys. Rev. C **56**, 1084 (1997).
- [12] For computations of the gluon spectrum to all orders in the density of the nucleus ($k_t \sim Q_s$) see Y. V. Kovchegov and A. H. Mueller, Nucl. Phys. B **529**, 451 (1998); A. Dumitru and L. McLerran, Nucl. Phys. A **700**, 492 (2002); A. Dumitru and J. Jalilian-Marian, Phys. Lett. B **547**, 15 (2002); J. P. Blaizot, F. Gelis and R. Venugopalan, Nucl. Phys. A **743**, 13 (2004).
- [13] For lattice computations of the gluon spectrum to all orders in the density of identical projectile and target see A. Krasnitz and R. Venugopalan, Nucl. Phys. **B557**, 237 (1999); Phys. Rev. Lett. **84**, 4309 (2000); Phys. Rev. Lett. **86**, 1717 (2001); A. Krasnitz, Y. Nara, and R. Venugopalan, Phys. Rev. Lett. **87**, 192302 (2001); Nucl. Phys. A **717**, 268 (2003); Nucl. Phys. A **727**, 427 (2003); T. Lappi, Phys. Rev. C **67**, 054903 (2003).
- [14] L. Frankfurt, V. Guzey, M. McDermott and M. Strikman, Phys. Rev. Lett. **87**, 192301 (2001).
- [15] J. Bartels, E. Gotsman, E. Levin, M. Lublinsky and U. Maor, Phys. Rev. D **68**, 054008 (2003).

- [16] E. A. Kuraev, L. N. Lipatov and V. S. Fadin, Sov. Phys. JETP **45**, 199 (1977) [Zh. Eksp. Teor. Fiz. **72**, 377 (1977)]; I. I. Balitsky and L. N. Lipatov, Sov. J. Nucl. Phys. **28**, 822 (1978) [Yad. Fiz. **28**, 1597 (1978)].
- [17] V. N. Gribov and L. N. Lipatov, Yad. Fiz. **15**, 781 (1972) [Sov. J. Nucl. Phys. **15**, 438 (1972)]; Yad. Fiz. **15**, 1218 (1972) [Sov. J. Nucl. Phys. **15**, 675 (1972)]; G. Altarelli and G. Parisi, Nucl. Phys. B **126**, 298 (1977); Yu. L. Dokshitzer, Sov. Phys. JETP **46**, 641 (1977) [Zh. Eksp. Teor. Fiz. **73**, 1216 (1977)]; Yu. L. Dokshitzer, D. Diakonov and S. I. Troian, Phys. Rept. **58**, 269 (1980).
- [18] A. H. Mueller and B. Patel, Nucl. Phys. B **425**, 471 (1994); J. Bartels, E. Gotsman, E. Levin, M. Lublinsky and U. Maor, Phys. Lett. B **556**, 114 (2003); E. Iancu and A. H. Mueller, Nucl. Phys. A **730**, 460 (2004); E. Levin and M. Lublinsky, Phys. Lett. B **607**, 131 (2005).
- [19] R. Baier, A. H. Mueller and D. Schiff, Nucl. Phys. A **741**, 358 (2004).
- [20] K. Rummukainen and H. Weigert, Nucl. Phys. A **739**, 183 (2004); H. Weigert, arXiv:hep-ph/0501087.
- [21] D. Kharzeev and E. Levin, Phys. Lett. B **523**, 79 (2001); D. Kharzeev, E. Levin and M. Nardi, Nucl. Phys. A **730**, 448 (2004) [Erratum-ibid. A **743**, 329 (2004)].
- [22] L. Frankfurt and M. Strikman, private communication.
- [23] J. Jalilian-Marian and Y. V. Kovchegov, Phys. Rev. D **70**, 114017 (2004) [Erratum-ibid. D **71**, 079901 (2005)].
- [24] A. Dumitru, A. Hayashigaki and J. Jalilian-Marian, to be published.
- [25] R. K. Ellis, W. J. Stirling and B. R. Webber, “QCD and Collider Physics”, Cambridge University Press, 1996.
- [26] The inverse Compton kinematics has been discussed first within the present context by S. Brodsky, talk given at the RIKEN-BNL Workshop on “High-pT Physics at RHIC”, December 2 – 6, 2003, Brookhaven National Laboratory, Upton, NY, USA,

http://quark.phy.bnl.gov/www/riken/highpt_03.html;
- L. Frankfurt, talk given at the 44th Workshop, INFN Eloisatron Project, “QCD at Cosmic Energies”, August 29 - September 5, 2004, Erice, Italy,

<http://www.lpthe.jussieu.fr/erice/>

and private communication.
- [27] H. L. Lai *et al.* [CTEQ Collaboration], Eur. Phys. J. C **12**, 375 (2000).
- [28] B. A. Kniehl, G. Kramer and B. Pötter, Nucl. Phys. B **582**, 514 (2000).

- [29] L. McLerran and R. Venugopalan, Phys. Rev. D **49**, 2233 (1994); *ibid.* **49**, 3352 (1994); Y. V. Kovchegov, *ibid.* **54**, 5463 (1996); *ibid.* **55**, 5445 (1997).
- [30] F. Gelis, unpublished; D. Boer and A. Dumitru, Phys. Lett. B **556**, 33 (2003); see also the paper by Iancu *et al.* in [5].
- [31] I. Arsene *et al.* [BRAHMS Collaboration], Phys. Rev. Lett. **93**, 242303 (2004).
- [32] P. Aurenche, M. Fontannaz, J. P. Guillet, B. A. Kniehl and M. Werlen, Eur. Phys. J. C **13**, 347 (2000).
- [33] A. Dumitru, L. Gerland and M. Strikman, Phys. Rev. Lett. **90**, 092301 (2003) [Erratum-*ibid.* **91**, 259901 (2003)].
- [34] E. Iancu, K. Itakura and S. Munier, Phys. Lett. B **590**, 199 (2004).
- [35] G. Rakness [STAR Collaboration], arXiv:hep-ex/0505062; hep-ex/0507093.